Dynamics within tetraspanin pairs affect MHC class II expression

Tineke van den Hoorn, Petra Paul, Lennert Janssen, Hans Janssen and Jacques Neefjes*

Division of Cell Biology, The Netherlands Cancer Institute, Plesmanlaan 121, 1066 CX Amsterdam, The Netherlands

*Author for correspondence (j.neefjes@nki.nl)

Accepted 11 August 2011
Journal of Cell Science 125, 328–339

doi: 10.1242/jcs.088047

Summary

Late endosomal multivesicular bodies (MVBs) are complicated organelles with various subdomains located at the limiting membrane and the internal vesicles (ILVs). ILVs accumulate tetraspanins such as CD63 and CD82 that might form protein assemblies, including major histocompatibility complex class II (MHC-II) and its chaperone human leukocyte antigen (HLA)-DM. Here, we studied the effect of four late endosomal tetraspanin proteins on MHC-II expression. Silencing CD9, CD63 and CD81 enhanced MHC-II expression whereas silencing CD82 did not. No effect on peptide loading was observed. Using confocal FRET technology, we measured the dynamics of CD63 and CD82 interaction with MHC-II and its chaperone HLA-DM. CD63–CD82 interactions remained unaltered in the two MVB subdomains whereas the interactions between CD63 or CD82 homologous pairs changed. CD63 stably associated with MHC-II, and CD82 with HLA-DM, on both MVB subdomains whereas the CD82–MHC-II and CD63–HLA-DM interactions changed. These data visualize for the first time the protein dynamics of tetraspanin assemblies in MVB subdomains. CD63, unlike CD82, stably interacts with MHC-II at both MVB subdomains and controls MHC-II expression.

Key words: FRET, HLA-DM, MHC class II, MVB, Tetraspanin, CD63, CD82

Introduction

MHC-II-enriched compartments (MIICs) are multivesicular bodies (MVBs) or multilamellar structures of acidic pH that contain major histocompatibility complex class II (MHC-II) and human leukocyte antigen (HLA)-DM molecules, as well as proteases (Neefjes, 1999). Their architecture is unique: a limiting membrane (LM) surrounds a large set of small vesicles termed intraluminal vesicles (ILVs) that might be generated by the ESCRT machinery (Teis et al., 2009). This machinery selects ubiquitin-tagged proteins for sorting into ILVs, resulting in a distinct composition of two subdomains of the same MVB, the ILV and the LM. Tetraspanins and other molecules, such as lipids like lyso-bis-phosphatidic acid (LBPA), concentrate in ILVs, whereas other proteins like LAMP1 are found predominantly on the LM (Griffiths et al., 1988). The intravesicular sorting of LBPA is not likely to be orchestrated by the ESCRT machinery and could be driven by alternative mechanisms.

MHC-II presents antigenic peptide fragments, acquired in the endocytic route, to the immune system. In humans, three MHC-II alleles exist named HLA-DR, HLA-DQ and HLA-DP. MHC-II consists of αβ-heterodimers that assemble in the endoplasmic reticulum (ER) with the invariant chain (Ii) polypeptide. Ii fills the peptide loading groove of MHC-II and targets MHC-II to late endosomal compartments, generally named MIIC (Neefjes et al., 1990; Roche and Cresswell, 1990; Peters et al., 1991). The ESCRT machinery is important for MIIC sorting and function, as shown by an siRNA screen for MHC-II peptide loading and expression that revealed many components of the ESCRT 0, I, II and III system (Paul et al., 2011). In the MIIC, Ii is degraded by resident proteases, except for a short fragment called CLIP that is protected by the surrounding peptide-binding groove. The chaperone HLA-DM also resides in MIIC and facilitates the exchange of CLIP for high-affinity binding peptides generated by resident proteases (Denzin and Cresswell, 1995; Kropshofer et al., 1997). Whereas MHC-II and HLA-DM are both found on the LM and ILV of MVBs, they interact predominantly in the ILV, as determined by fluorescence resonance energy transfer (FRET) experiments (Zwart et al., 2005).

It is unclear why MHC-II fails to interact with HLA-DM at the LM of MIIC. One possibility is that tetraspanin proteins or networks concentrate these molecules and stabilize their interaction. The tetraspanins CD63 and CD82 are enriched in ILVs (Escola et al., 1998) and form complexes with HLA-DR, HLA-DM and HLA-DO molecules, as detected by biochemical experiments (Hammond et al., 1998; Engering and Pieters, 2001), but the biological consequences of these interactions are unclear.

Tetraspanins probably form supramolecular complexes or microdomains, also called tetraspanin-web (Rubinstein et al., 1996). Cryo-electron microscopy studies showed that tetraspanins can assemble into highly regular protein complexes. Tetraspanins might organize other proteins into these supramolecular webs to facilitate protein interactions (Min et al., 2006).

We hypothesized that tetraspanins on ILV act as a MHC-II peptide-loading platform by stabilizing interactions between MHC-II and HLA-DM. We silenced four tetraspanin proteins located in the MVB (CD9, CD63, CD81 and CD82) and determined the effect on MHC-II expression and peptide loading, using flow cytometry as described before (Paul et al., 2011). All but the CD82 tetraspanin appeared to control MHC-II expression, although silencing the tetraspanin proteins did not prevent peptide loading. We selected one tetraspanin (CD63) that controls MHC-II expression and one (CD82) that does not affect

Journal of Cell Science

it. Using FRET technology, we assayed the CD63 and CD82 interactions in the tetraspanin networks and interactions with MHC-II and HLA-DM in the LM and ILV of the same MVB. After verification of correct localization of the fluorescently tagged molecules by immuno-electron microscopy, we performed confocal FRET (van Rheenen et al., 2004) on vesicles. These were neutralized and expanded by chloroquine treatment because MVBs are too small to distinguish LM from ILV by light microscopy on living unfixed cells (Zwart et al., 2005). We tested various combinations of MHC-II and HLA-DM with CD63 and CD82 to show that the orientation of CD63 and CD82 alters in the two different MVB domains, as does their interaction with MHC-II and HLA-DM. These experiments are the first to reveal the dynamics of interactions within the tetraspanin web on subdomains in one compartment, the late endosomal MVB. These data suggest a model of dynamic and selective interactions of tetraspanins with associated molecules HLA-DM and MHC-II within MVB subdomains, which might also occur for other tetraspanin-associated proteins. The stable expression of CD63 (but not CD82) with MHC-II might explain the selective effect of increased MHC-II expression following CD63 silencing.

Results

Tetraspanin proteins and MHC-II expression

Four different late endosomal tetraspanin proteins (CD63, CD81, CD82 and CD9) have been shown to interact with MHC-II and HLA-DM in biochemical experiments. To define the effect of tetraspanin proteins on MHC-II loading and expression, we silenced these in the MHC-II-expressing cell line MelJuSo using RNA interference. Because siRNA might also affect the mRNA levels of other genes, we used quantitative RT-PCR (qPCR) to check the influence of the different siRNAs and control siRNAs on the mRNA expression of HLA-DRα and the various tetraspanins (Fig. 1A). All tetraspanins were silenced by more than 70–80% whereas expression of mRNA encoding HLA-DRα-chain was increased following silencing of HLA-DM and CD9 only. We checked whether silencing of a defined tetraspanin would result in compensation by another tetraspanin. We determined the mRNA expression of all tetraspanins in MelJuSo cells in which HLA-DM or one of the tetraspanins was silenced (Fig. 1A, right panel). Silencing HLA-DM decreased the levels of all tetraspanins tested. Silencing of CD82 was compensated by higher expression of CD9, whose knockdown in turn led to decreased expression of all other genes tested. The siRNAs targeting other tetraspanins only had marginal off-target effects.

We investigated the effect of silencing tetraspanins on cell surface MHC-II expression and peptide loading using antibodies detecting proper peptide-loaded MHC-II (antibody L243) and Ii-fragment CLIP-loaded MHC-II (antibody CerCLIP), as described previously (Paul et al., 2011). Silencing CD9, CD63 and CD81 increased MHC-II expression, whereas no effect was detected when CD82 was silenced. Silencing these tetraspanins did not affect peptide loading as detected by CerCLIP (HLA-DM was included as a positive control). To control whether silencing of the tetraspanin alters the intracellular MHC-II distribution, MelJuSo cells were again transfected with the different siRNAs, fixed and stained 6 days later for MHC-II and LAMP2 (a marker for late endosomes) (Fig. 1C). No detectable differences in LAMP2 and MHC-II distribution were observed after silencing HLA-DM or any of the tetraspanins. These data suggest a role of three tetraspanin proteins in the control of MHC-II expression. Because the qPCR data show that MHC-II expression is not controlled at the transcriptional level, the tetraspanins apparently control a post-translational step such as the release from tetraspanin networks in late endosomes. CD82 interacts with MHC-II, HLA-DM and CD63 in biochemical experiments but does not control MHC-II expression. Next, we studied in detail the role of CD63 (one of three tetraspanins controlling MHC-II expression) and CD82 in interactions between tetraspanins or with HLA-DM and MHC-II in subdomains of the MVB.

Reconstituting expression of MHC-II and tetraspanins in HEK293T cells

MHC-II expression is limited to antigen presenting cells (APC), such as dendritic cells, macrophages, B-cells and monocytes. These primary immune cells are difficult to manipulate genetically and are photosensitive, which complicates live-cell fluorescence microscopy. We therefore reconstituted a cellular model system by stably expressing the relevant molecules in human embryonic kidney (HEK) cells. HEK293T cells were used to introduce Ii along with YFP-tagged MHC-II HLA-DRB3 (with non-fluorescent HLA-DRA) alone or in combination with CFP-tagged HLA-DM. To show proper formation of MHC-II complexes, we performed flow cytometry using L243 and CerCLIP antibodies and compared the expression with the endogenously MHC-II-expressing melanoma cell line MelJuSo (Fig. 2A). MHC-II molecules were efficiently expressed and presented CLIP fragments when HLA-DM was absent, as described before (Avva and Cresswell, 1994).

We also introduced CFP- or YFP-tagged CD63 or CD82 molecules into HEK293T cells. The tetraspanins were C-terminally tagged to avoid interference with the lysosomal targeting signal (Blott et al., 2001). Localization of endogenously or ectopically expressed fluorescently tagged tetraspanins was determined by confocal laser scanning microscopy (CLSM) and electron microscopy (Fig. 2B). Similarly to endogenous tetraspanins, YFP–CD63 and YFP–CD82 localized to intracellular compartments and to the cell surface. To determine the relative expression levels of endogenous versus ectopic CD63 or CD82, we analyzed the cells by SDS-PAGE and western blotting, considering the additional molecular weight contributed by the YFP tag (Fig. 2C). Tetraspanins have extensive carbohydrate chains, which generate multiple bands in SDS-PAGE. Still, ectopically expressed YFP–CD63 constitutes more than half of the total CD63 pool, and the ectopic CD82 pool constitutes considerably more than the endogenous CD82 expressed in HEK293T cells. Relatively high expression of CFP- or YFP-tagged molecules over endogenous molecules is essential to achieve a reasonable amount of fluorescent pairs for FRET detection because pairing with endogenous non-fluorescent molecules will quench the FRET signal.

We thus created model cells to study the dynamics of MHC-II and HLA-DM interactions within the context of tetraspanin complexes in the MVB of living cells.

Lateral movement of tetraspanins and HLA-DR in the plasma membrane

Proteins diffuse in lipid bilayers at rates dependent on their radius in the membrane according to the Saffman–Delbruck equation, $D=cT\ln[(k/\eta a)-0.05772]$, where D is diffusion in the membrane, c and k are constants, T is absolute temperature, η is viscosity of the membrane and a is the radius of the transmembrane segments (Saffman and Delbruck, 1975; Reits

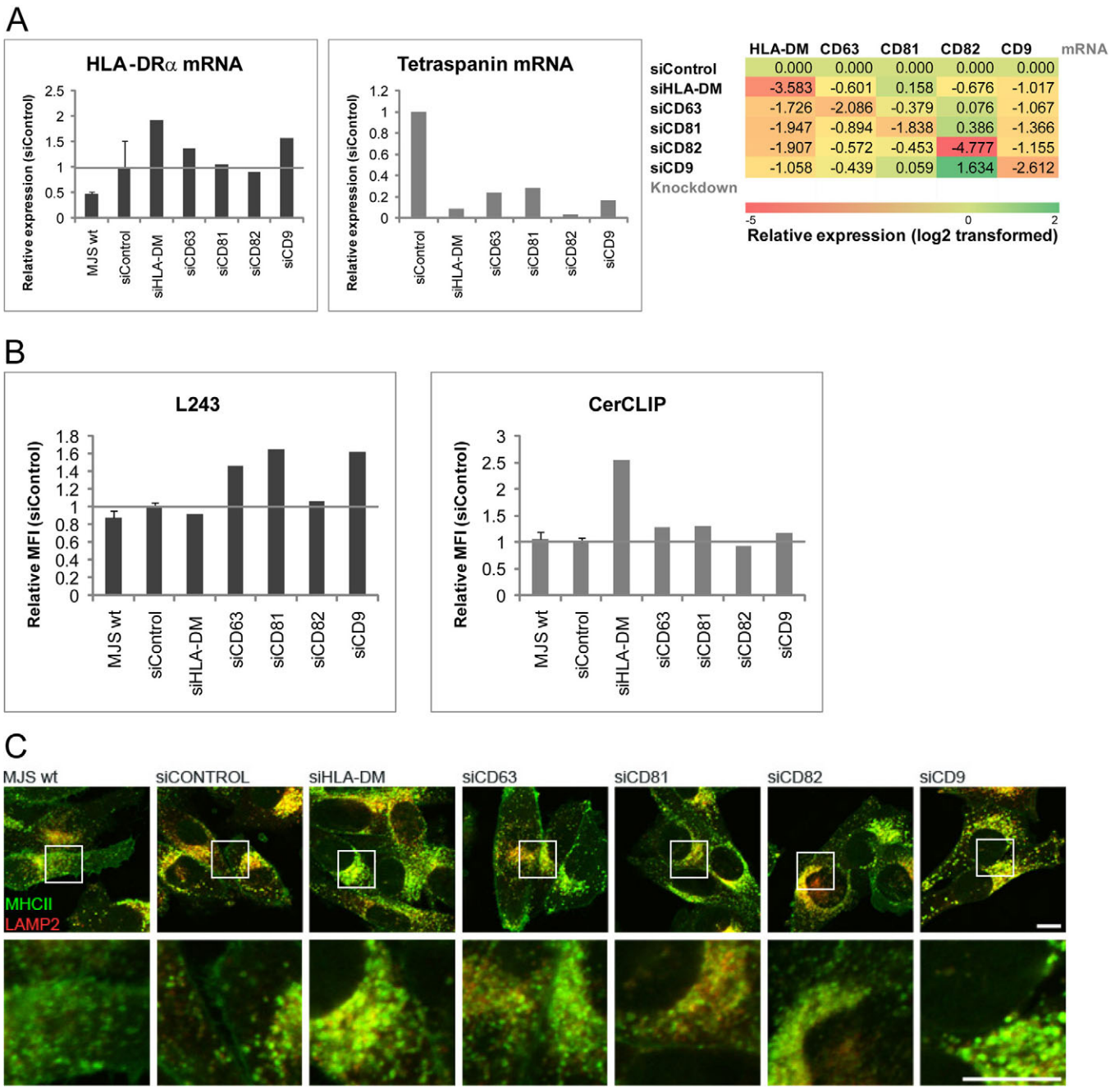

Fig. 1. Tetraspanins and MHC-II expression and peptide loading. (**A**) Effect of siRNA-mediated silencing of tetraspanins on levels of mRNAs encoding HLA-DR or tetraspanin. MelJuSo cells were transfected with non-targeting siRNA (siControl), or siRNA against HLA-DM or the tetraspanins CD9, CD63, CD81 or CD82. At 3 days post-transfection, mRNA was isolated for qPCR. The results were normalized to the values obtained for the siControl. Left panel: normalized qPCR data for *HLA-DRα* mRNA. Middle panel: normalized qPCR data for the direct targets of the siRNAs. Right panel: qPCR to test for compensation by other tetraspanins. Values are normalized to the siControl and log2 transformed. Decrease is shown in red and upregulation in green. (**B**) MelJuSo cells were transfected with the siRNAs indicated for 6 days before analysis by flow cytometry for MHC-II expression (L243) and peptide loading (CerCLIP). The mean fluorescence intensity (MFI) was normalized to the value obtained in cells transfected with siControl. (**C**) Effect of silencing tetraspanins on MHC-II and LAMP2 distribution. MelJuSo cells were transfected with the siRNAs indicated for 6 days, fixed and stained for MHC-II (green) and late endosomal marker LAMP2 (red). A zoom-in is shown below each image (white box in upper image). Scale bars: 10 μm.

and Neefjes, 2001). Consequently, large protein complexes (such as tetraspanins) diffuse slower than smaller ones unless interacting with larger complexes that are less mobile, as can be assessed by fluorescence recovery after photobleaching (FRAP) (Reits and Neefjes, 2001).

Tetraspanins have four transmembrane regions and might assemble into large protein networks, which would result in slow lateral mobility. Peptide- or CLIP-loaded MHC-II HLA-DR3–YFP complexes contain two transmembrane regions. MHC-I HLA-A2–GFP (introduced as a control molecule) contains one

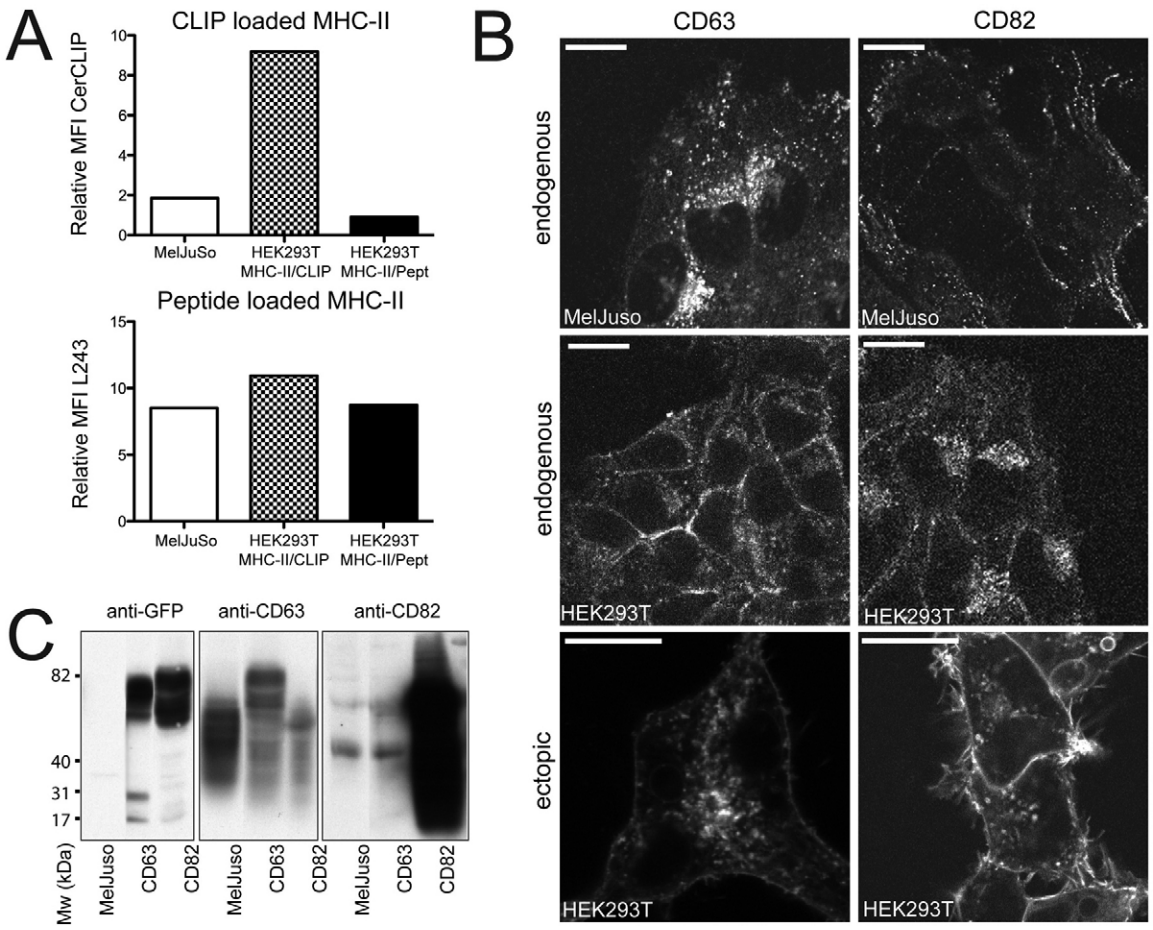

Fig. 2. Characterization of MHC-II peptide loading and tetraspanin FRET pair expression in HEK293T cells. (**A**) Cell surface expression of CLIP-loaded MHC-II (detected by CerCLIP antibody) and peptide-loaded MHC-II (detected by L243 antibody) on MelJuSo and HEK293T cells stably expressing MHC-II (HLA-DRα, HLA-DRβ–YFP, Ii) in the absence (HEK293T MHC-II/CLIP) or presence (HEK293T MHC-II/Pept) of HLA-DM–CFP, as measured by flow-cytometry. Depicted is the mean fluorescence intensity (MFI) relative to secondary antibody only. (**B**) Distribution of endogenous and YFP-tagged tetraspanins. MelJuSo and HEK293T cells were stained for endogenous CD63 and CD82, or YFP–CD63 and YFP–CD82 were detected by CLSM. (**C**) Biochemical analyses of HEK293T cells expressing CFP– and YFP–CD63 (CD63) or CFP– and YFP–CD82 (CD82). Lysates of the transfectants CD63 and CD82 (and MelJuSo cells as control) were separated by SDS-PAGE and the western blot incubated with anti-CD63, anti-CD82 or anti-GFP (recognizing YFP and CFP tags) antibodies, as indicated. The position of the molecular mass (Mw) standard is indicated. Scale bars: 20 μm.

transmembrane region only (Gromme et al., 1999). We performed FRAP experiments on HEK293T cells expressing YFP–CD63, YFP–CD82, CLIP-loaded HLA-DRB–YFP and peptide-loaded HLA-DRB–YFP. Both peptide- and CLIP-loaded MHC-II moved considerably slower than MHC-I, and diffused at rates similar to CD63 or CD82. These results cannot be directly compared with other reported diffusion rates because the temperature and viscosity of the cells used might differ, with major effects on diffusion rates. The immobile fraction for MHC-I was smaller than for MHC-II or tetraspanins (Fig. 3B,C). This suggests that MHC-II resides in larger protein complexes at the plasma membrane than MHC-I. These complexes might contain tetraspanins that have similar diffusion characteristics in living cells. However, as diffusion might be determined by many associating complexes or domains, we cannot conclude anything about specific protein–protein complexes. This requires FRET technology, where the distance and orientation of two fluorophores is directly measured.

Considerations on FRET studies of proteins in the MVB

To visualize the incorporation of HLA-DR and HLA-DM into tetraspanin webs containing CD63 and CD82, we measured FRET between the CFP- and YFP-tagged molecules in various combinations. When two fluorophores are within a distance of approximately 100 Å, which usually implies direct interaction, FRET can be detected. Collisional FRET can occur by excessive overexpression of two fluorescently tagged proteins. We performed immuno-electron microscopy to assess antigen density. Results from double labelling of fluorescently tagged tetraspanins (anti-GFP) versus the total pool of CD63 or CD82 (anti-CD63 or anti-CD82) did not concur with excessive overexpression of fluorescently tagged tetraspanins compared with endogenously expressed tetraspanins (Fig. 4). In addition, labelling of MHC-II (anti-DR) and HLA-DM (anti-HLA-DM) in the HEK293T transfectants suggested modest ectopic expression levels (Fig. 4). The observed labelling intensities (even considering a detection efficiency of approximately 10% in

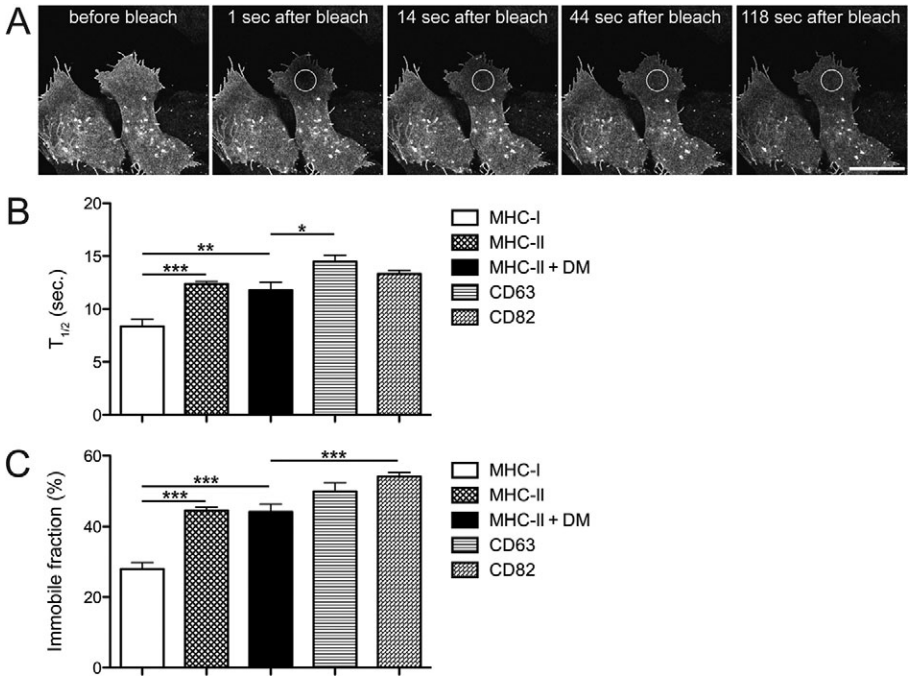

Fig. 3. Mobility of fluorescently tagged MHC-I (HLA-A2), MHC-II (HLA-DR3), CD63 and CD82 at the plasma membrane. HEK293T cells stably expressing CFP-, GFP- or YFP-tagged MHC-I and MHC-II (with or without coexpression of HLA-DM, CD63 or CD82) were bleached according to the FRAP protocol to determine the mobility and the mobile fraction of these fluorescent proteins at the plasma membrane. (**A**) HEK293T cells expressing YFP–CD63 imaged before, at, and several time points after point bleach. Fluorescence recovery is measured in a region of interest (ROI) represented by the white ring. Scale bar: 20 μm. (**B**) Mean mobility as $T_{1/2}$ values (seconds) and (**C**) immobile fractions (percentage of initial fluorescence in the bleach spot) for fluorescently tagged MHC-I ($n=15$), MHC-II ($n=33$), MHC-II in the presence of HLA-DM ($n=12$), YFP–CD63 ($n=27$) and YFP–CD82 ($n=22$) expressed in HEK293T cells. Error bars represent s.e.m. *$P<0.05$, **$P<0.01$, ***$P<0.001$ (Student's t-test).

electron microscopy slides) and the fact that the CFP- and YFP-tagged molecules did not show any clustering in the fixed electron microscopy sections, suggests that collision FRET is not a major factor contributing to our detected signals. Of note, our aim was to detect relative alterations in FRET when molecules redistribute within one MVB, and such differences would not concur with collision as an explanation for FRET signals. FRET is highly sensitive to the distance as well as to the orientation of the two fluorophores. This implies that differences in FRET do not necessarily reflect differences in distance, but could equally well indicate an altered orientation of the fluorescent tags or a combination of the two. However, a bona fide FRET signal always reflects close local distance between two molecules.

Expanding MVBs for distinguishing LM and ILV by light microscopy

To determine FRET on membranes of MBV, high resolution data were collected using CSLM followed by calculation of sensitized emission FRET (seFRET) (van Rheenen et al., 2004). MVBs containing MHC-II and HLA-DM are around 400 nm in diameter, which does not allow separation of ILV and LM within these structures by conventional light microscopy. To overcome this, cells were exposed to chloroquine, which neutralizes and swells the MVB (Zwart et al., 2005). For swelling to occur, lipids have to arrive at the LM (a membrane cannot become thinner 'like a balloon'). To test whether membranes required for swelling are derived from new vesicles or from within the MVB (by back-fusion of ILV), we first exposed HEK293T cells expressing GFP–CD63 to chloroquine, which induced the formation of swollen structures (Fig. 4A). This experiment was repeated in the presence of nocodazole, which eliminates microtubules to effectively prevent vesicle transport. Chloroquine expanded the MVB, implying that the membranes for swelling are not delivered by other vesicles (Fig. 4A). To further test the origin of materials required for vesicle expansion, the location of CFP- or YFP-labelled proteins were defined on expanded structures by immuno-electron microscopy. Sections of HEK293T (with or without chloroquine treatment) expressing the tetraspanins and MHC-II or HLA-DM were labelled with anti-GFP antibodies and further probed with gold particles (Fig. 4B). The ILV of most MVBs were labelled for the proteins indicated, and chloroquine exposure yielded swollen structures with internal vesicles still labelled for the CFP- and YFP-tagged proteins. Yet, these molecules moved from ILV to the LM in chloroquine-expanded MVBs, as visible by confocal microscopy (Fig. 4A) as well as by immuno-electron microscopy (Fig. 4B) (Zwart et al., 2005). These data suggest that expansion of the LM of swollen MVBs by chloroquine exposure is the result of back-fusion of ILV to the LM of MVBs. This process provides the membranes required for the expansion of the LM.

Swelling of MVBs is a relatively slow process. After exposure of cells to chloroquine for 3 hours, the MVBs were partially swollen, with some ILV still present in the expanded MVB. After 6 hours of exposure to chloroquine, MVBs were fully expanded without any detectable ILV left, as extensively shown for 293T cells previously (Zwart et al., 2005).

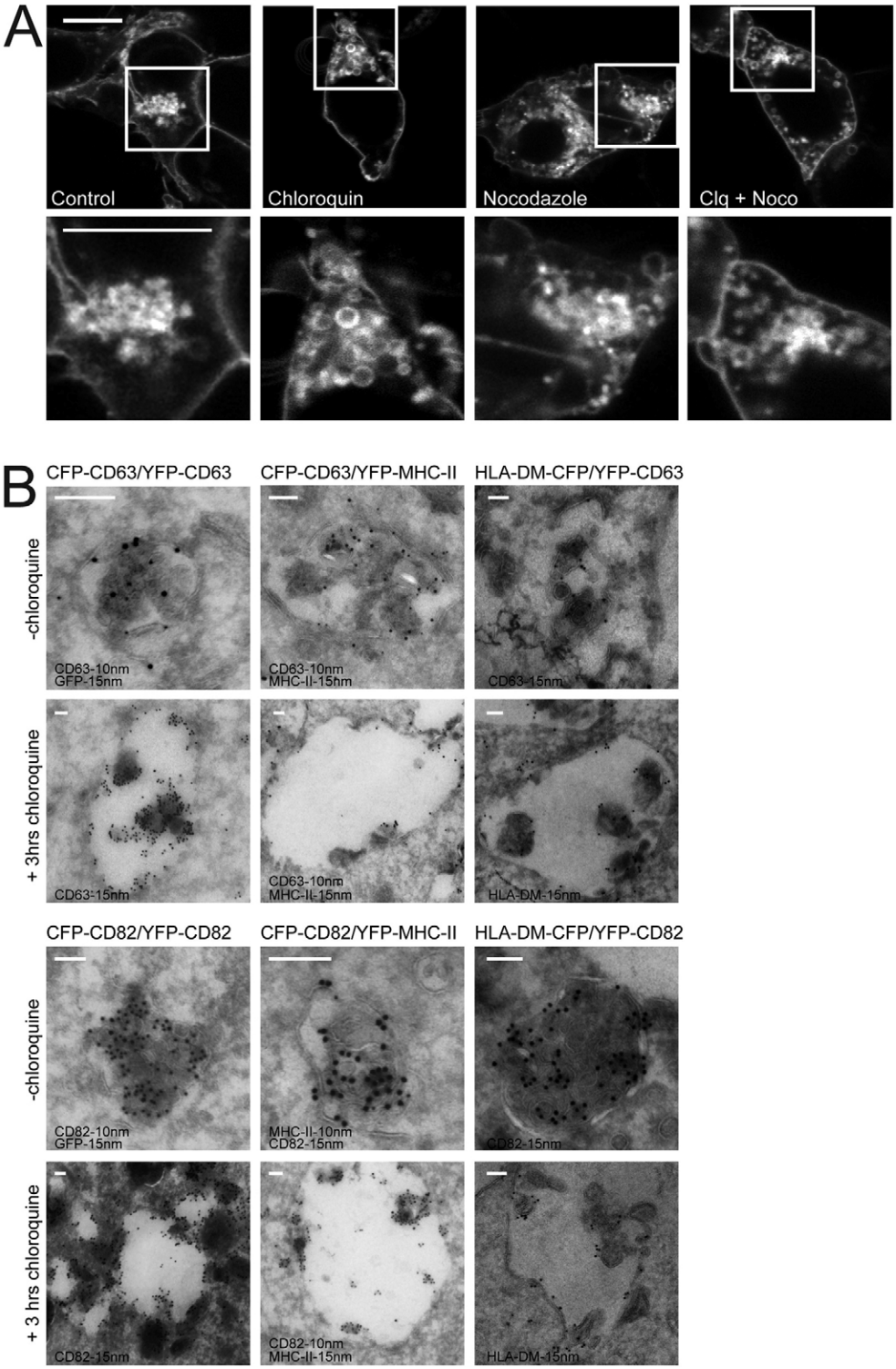

Fig. 4. Expansion of MVBs and distribution of CFP- or YFP-tagged proteins. (**A**) Live confocal images of HEK293T cells expressing GFP–CD63 treated with 100 μM chloroquine for 3 hours in the presence or absence of chloroquin and/or nocodazole to disrupt microtubular transport. Bottom panel: zoom-in of white box in top panel. Scale bars: 10 μm. (**B**) Electron micrographs of stable HEK293T cell transfectants expressing YFP– and CFP–CD63, YFP– and CFP–CD82, CFP–CD63 or CFP–CD82 together with MHC-II–YFP and HLA-DM–CFP together with YFP–CD63 or YFP–CD82, as indicated. Cells were fixed before (–) or after 3 hours of chloroquine treatment and cryosections stained with anti-GFP, anti-CD63, anti-CD82, anti-HLA-DM and anti-HLA-DR antibodies and gold particles for detection by electron microscopy, as indicated. Representative images of control or chloroquine-treated (partially swollen) MVBs are shown. Scale bars: 200 nm.

Controls for FRET signals under chloroquine exposure

To investigate whether MHC-II and HLA-DM reside in tetraspanin networks containing CD63 and CD82, we generated cells with different combinations of tetraspanins and MHC-II or HLA-DM molecules. The fluorescent tag always localizes to the cytosol or the interior of ILV (which are topologically identical). Because we have to manipulate the cells with chloroquine to expand the MVB for analyses by CLSM, we tested the effects of chloroquine on FRET between CD63 and CD82. Chloroquine diffuses almost instantaneously over membranes, causing neutralization of acidic compartments including the MVB (Zwart et al., 2005). We exposed cells to chloroquine for 10 minutes (when MVB swelling is not detected) before FRET was measured. Neutralization of the MVB by chloroquine only

had small effects on FRET values between the protein pairs tested. For instance, FRET values between a fluorescently tagged CD82–CD82 pair showed a subtle increase, whereas only a small decrease for the fluorescently tagged CD63–CD63 pair was observed following neutralization of MVBs (Fig. 5A). Because chloroquine exposure yielded different effects for the various FRET pairs tested, the effects are not due to pH (which is clamped by chloroquine at ~pH 7.0), but indicate pH-dependent reorganization of complexes. To compensate for the effects of pH on FRET values between our protein pairs, we related FRET values measured on swollen MVBs to FRET values obtained after cells had been exposed to chloroquine for 10 minutes.

Controlling vesicle movement for accurate confocal FRET measurements

For confocal FRET measurements, the sample is excited by light at 430 nm and donor fluorescence and acceptor fluorescence (the actual FRET) emission is measured. This is followed by excitation with light of 514 nm to measure acceptor fluorescence emission. From these three data sets, FRET and donor FRET efficiency (E_D, FRET related to donor fluorescence) can be calculated. Because we work at maximal microscopy resolution, the MVBs in the living cells should not move between the images made for determining FRET (which takes ~5 milliseconds) as we calculate the amount of signal per pixel. Chemical fixation is no alternative because fixation will unpredictably affect the protein complexes. Immediate elimination of all microtubule-based transport by high concentrations of nocodazole was not sufficient (the vesicles still showed some 'trembling'; not shown)

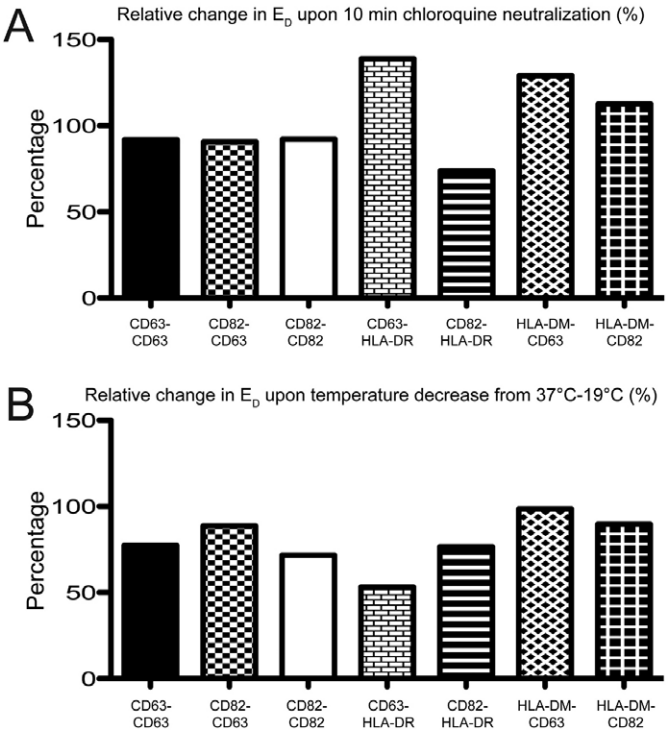

Fig. 5. Effects of chloroquine addition and temperature decrease on FRET E_D values. (**A**) Neutralization by incubation with chloroquine for 10 minutes had various effects on E_D for the different pairs measured (control situation of 19℃, without chloroquine, is set to 100%). (**B**) Change in temperature from 37℃ to 19℃ also decreases the E_D (37℃ is set as 100%).

and apoptosis of the cells was induced after prolonged culture.

We then decided to perform FRET measurements on cells at 19℃ instead of 37℃. We monitored vesicle motion at different temperatures and detected sufficient quenching of vesicle motion at temperatures below 19℃ to allow adequate and reliable FRET measurements at our level of resolution. To test whether FRET is affected by lowering the temperature, we measured FRET between CFP–CD63 and YFP–CD63 at temperatures between 19℃ and 37℃, and observed only small effects on FRET (Fig. 5B). FRET measurements of living cells at 19℃ yielded more accurate data at high magnification with minor effects on calculated FRET values. We used this condition to measure differences in FRET between tetraspanin proteins CD63 and CD82 as well as with the interacting proteins HLA-DM and MHC-II.

We thus defined a protocol that should enable FRET determination within living cells at a resolution distinguishing ILV from LM within the MVB: (1) CLSM data for FRET determination were acquired at 19℃. FRET values were calculated as described (van Rheenen et al., 2004). (2) Discrimination between MVBs either containing or lacking ILV (mainly consisting of LM) was achieved by comparing FRET on vesicles in cells exposed to chloroquine for 10 minutes (normal ILV-containing neutral MVBs) or 6 hours (maximally expanded MVBs without ILV), respectively.

These conditions were used for data acquisition, allowing statistically sound statements. For illustration of the presentation of the measurements, Figs 4–6 show images of cells exposed to chloroquine for 3 hours, yielding partially swollen MVBs with some internal vesicles sufficiently separated from the LM for detection by CLSM and FRET determination.

CD63 and CD82 form homo- and heteromeric interactions in vivo

Applying the methods and considerations described above, we measured FRET between CFP- and YFP-tagged CD63 or CD82 molecules and between CFP–CD63 and YFP–CD82 molecules stably expressed in HEK293T cells. Sensitized emission FRET was determined and related to the donor fluorescence yielding donor FRET efficiency, E_D. Whereas E_D of the CD63–CD82 pair was similar at ILV and the LM, E_D was increased for the CD63–CD63 and CD82–CD82 pairs at the LM of the expanded MVBs (Fig. 6). These data suggest that the CD63–CD82 core is unaltered at limiting and internal membranes of MVBs, whereas CD63–CD63 and CD82–CD82 pairs reposition at the LM of an expanded MVB. Although the exact repositioning in molecular terms cannot be deduced from FRET studies, because the selective contribution of distance and orientation cannot be separated, these results show that tetraspanin networks are dynamic within one structure, the MVB.

Tetraspanin CD63, unlike CD82, stably interacts with MHC-II HLA-DR at LM and ILV

HLA-DR interacts with various tetraspanins, including CD63 and CD82, in biochemical studies (Hammond et al., 1998; Tarrant et al., 2003). To verify this interaction in living cells and to determine spatial differences within the MVB, CFP–CD63 or CFP–CD82 were coexpressed with YFP–MHC-II (HLA-DR3), and non-fluorescent Ii and HLA-DM in HEK293T cells. Donor FRET efficiency (E_D) was determined on MVBs of HEK293T

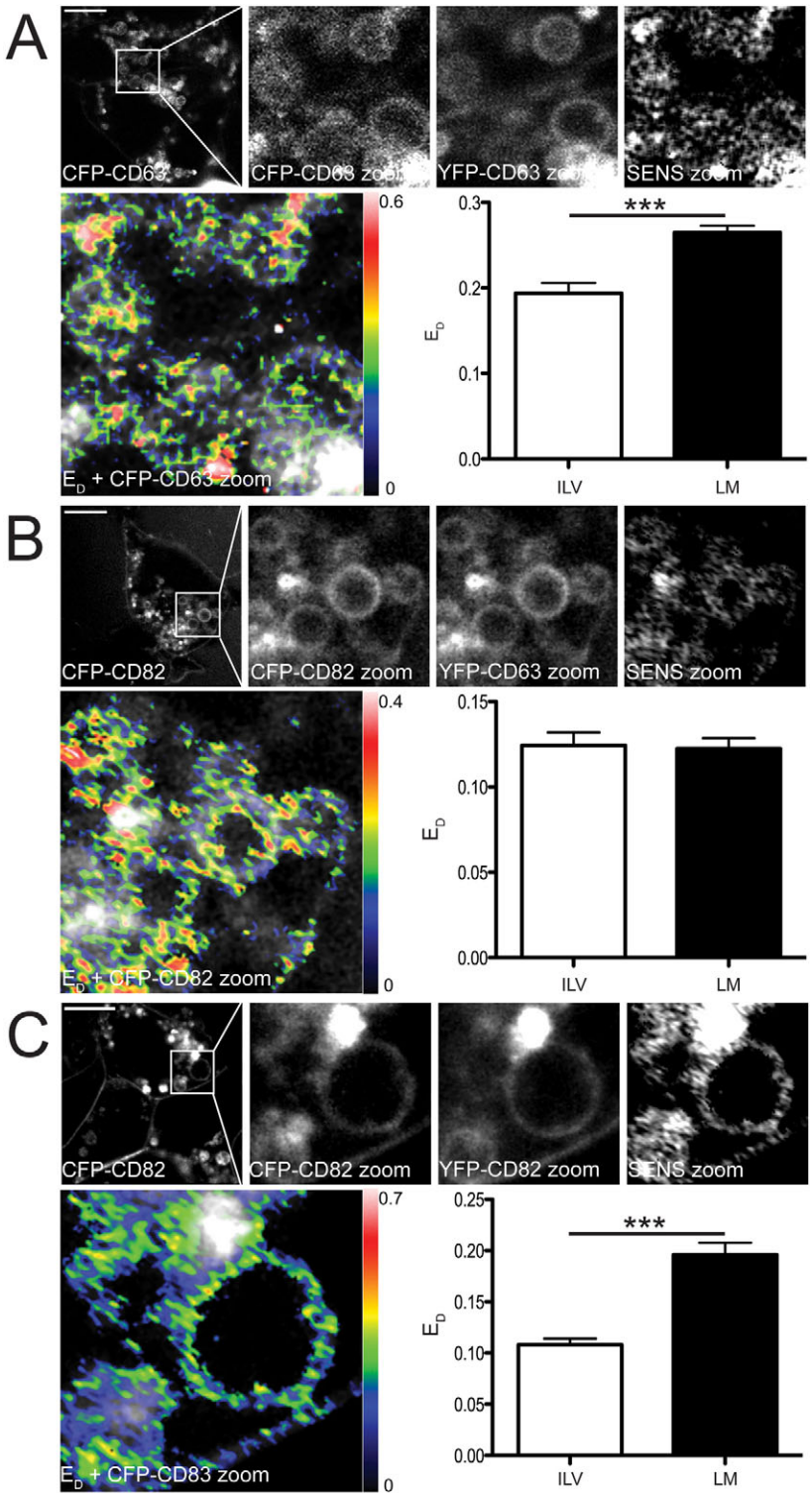

Fig. 6. seFRET between fluorescently tagged CD63 and CD82 combinations. (**A–C**) seFRET was measured in HEK293T cells stably expressing different combinations of CFP- and YFP-tagged CD63 and CD82. Microscopy images represent HEK293T cells with expanded MVBs to discriminate ILV and LM at 3 hours after chloroquine exposure. Top left images in A–C show overview of CFP images with zoom-in for CFP and YFP channel, as indicated. The SENS zoom images indicate the calculated seFRET after leak-through correction. The overlays show the calculated donor FRET efficiency E_D in rainbow colours (rainbow bar at right) representing the E_D values per pixel and projected onto the zoom-in of the CFP channel in white colours. The bar diagrams indicate the calculated E_D values for the interactions between the different tetraspanins at the LV (after 10 minutes of chloroquine) and LM (after 6 hours of chloroquine). (A) CFP–CD63 and YFP–CD63 pair; $n=129$ for ILV and $n=59$ for LM. (B) CFP–CD82 and YFP–CD63 pair: n(ILV)=9; n(LM)=34. (C) CFP–CD82 and YFP–CD82 pair: n(ILV)=43 and n(LM)=73. Error bars represent s.e.m. ***$P<0.001$ (Student's t-test). Scale bars: 10 µm.

cells exposed to chloroquine for 10 minutes (ILV) or 6 hours (LM; Fig. 7). The CD63–MHC-II interaction was unaltered between the two states, whereas the CD82–MHC-II interaction observed on the LM collapsed at the ILV. An expanded MVB imaged after 3 hours of chloroquine incubation illustrates the detected differences in E_D for ILV and LM within one MVB (Fig. 7). These MVBs still contain some internal structures, as detected in the zoom-ins of the CFP and YFP channels and the projection of E_D (in rainbow colours) on the CFP image (in white). Most internal vesicles containing CD82 and MHC-II did not yield any E_D signal, in accordance with the quantification of E_D for the two states of MVBs. These results indicate that HLA-DR interacts with CD63

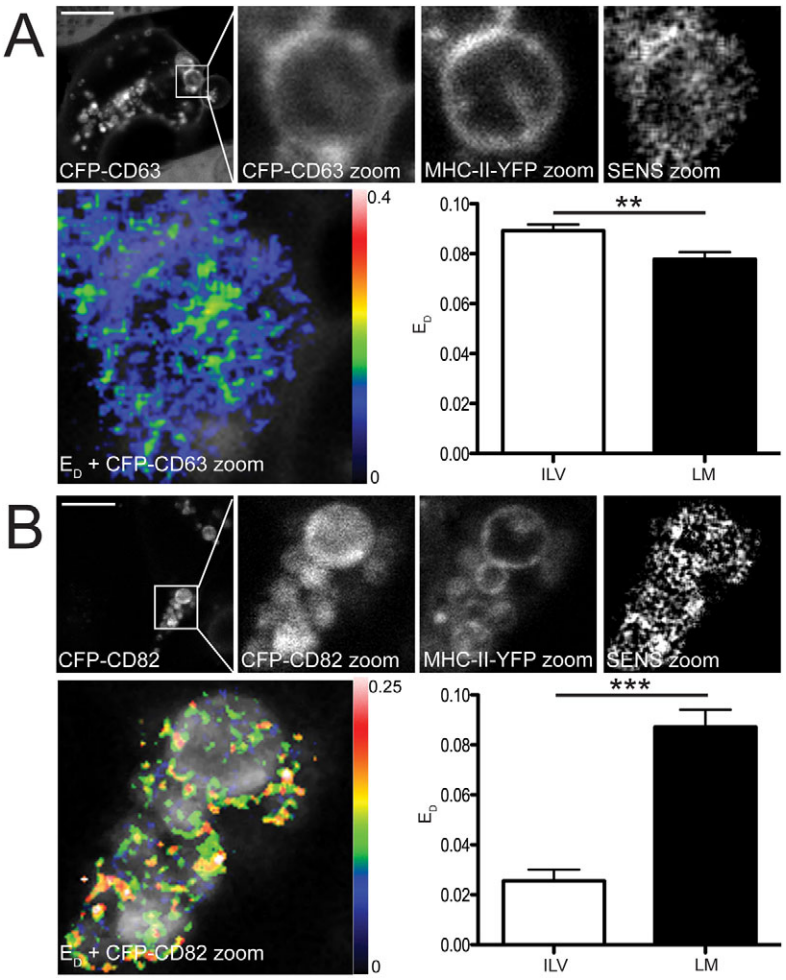

Fig. 7. seFRET between HLA-DRB3–YFP and tetraspanins CFP–CD63 or CFP–CD82. (**A**,**B**) FRET measurements and detection were as described for Fig. 6, but for HEK293T cells stably expressing the FRET pairs CFP–CD63 and MHC-II–YFP (A) or CFP–CD82 and MHC-II–YFP (B). In addition, Ii and HLA-DM lacking a fluorescent tag were overexpressed in these cells. Calculated E_D values are shown in the bar graphs. (A) CFP–CD63 and MHC-II–YFP pair: n(ILV)=127 and n(LM)=158. (B) CFP–CD82 and MHC-II–YFP pair: n(ILV)=43 and n(LM)=73. Error bars represent s.e.m. $^{**}P<0.01$, $^{***}P<0.001$ (Student's t-test). Scale bars: 10 µm.

on both domains of the MVB, whereas CD82 re-orientates or enters the network at the LM of MVBs only.

Tetraspanin CD82 – unlike CD63 – stably interacts with HLA-DM at LM and ILV

Because HLA-DM and MHC-II primarily pair at the ILV (Zwart et al., 2005), we wondered how HLA-DM would interact with the tetraspanins CD63 and CD82 at ILV and LM. We expressed CFP-tagged HLA-DM and YFP–CD63 or YFP–CD82 in HEK293T cells and measured E_D on chloroquine-control or chloroquine-expanded MVB (Fig. 8). CD82 associated with HLA-DM in a stable fashion and equal orientation, whereas CD63 yielded highest E_D in the ILV, rather than the LM of MVBs. This situation differed considerably from the interaction of tetraspanins with MHC-II, which stably interacted with CD63, whereas CD82–MHC-II interaction was only observed at the LM of MVBs (Fig. 7). The data suggest reorientation of MHC-II and HLA-DM within the reorganized tetraspanin network between ILV and LM of one MVB.

Discussion

The family of tetraspanin proteins is fascinating because they are major constituents of endosomes and still poorly understood. At least six tetraspanin proteins (including CD63 and CD82) are located in the late endosomal MVB, are enriched in the ILV (Peters et al., 1991; Escola et al., 1998; Wubbolts et al., 2003) and can be co-isolated with MHC-II and HLA-DM residing in the MVB (Hammond et al., 1998). In mouse dendritic cells, the tetraspanin molecule CD9 clusters with two types of MHC-II molecules, I-A and I-E, that show a distinct organization on the plasma membrane (Unternaehrer et al., 2007). This probably involves the C-terminal region of CD9 (Wang et al., 2011). Because tetraspanins accumulate at ILV and interact with both MHC-II and HLA-DM, the tetraspanin assemblies could act as a stabilizing factor. We tested this by silencing four tetraspanins that reside in the MVB and monitoring MHC-II peptide loading and cell surface expression. Three of the four tetraspanins controlled MHC-II cell surface expression but no effect on peptide loading was observed. In the FRET experiments, we focussed on the interactions of CD63 (which affects MHC-II expression) and CD82 (which does not affect MHC-II expression).

Whether CD63 and CD82 form pairs that dynamically interact with HLA-DM and MHC-II was investigated. FRAP experiments showed that MHC-II moves at a mobility comparable to CD63 and CD82 and more slowly than MHC-I. This suggests that MHC-II moves in association with these tetraspanins, but diffusion studies cannot provide information on this. Such conclusions can be drawn from FRET experiments because FRET is only detectable when two fluorophores are correctly

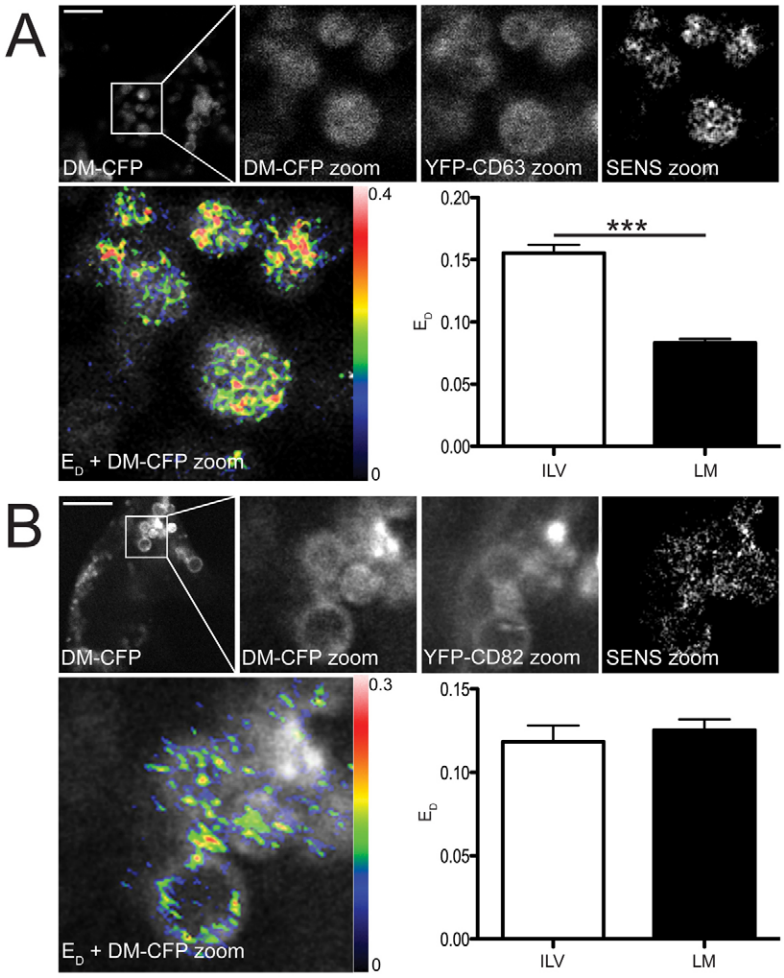

Fig. 8. seFRET between CFP–HLA-DM and tetraspanins YFP–CD63 or YFP–CD82. (**A**,**B**) FRET measurements and detection were as for Figs 6 and 7, but with HEK293T cells expressing the FRET pairs YFP–CD63 and HLA-DM–CFP (A) or YFP–CD82 and HLA-DM–CFP (B). Calculated E_D values are shown in the bar graphs. (A) HLA-DM–CFP and YFP–CD63 pair; n(ILV)=80 and n(LM)=111. (B) HLA-DM–CFP and YFP–CD82 pair: n(ILV)=49 and n(LM)=96. Error bars represent s.e.m. ***$P<0.001$ (Student's t-test). Scale bars: 10 µm.

positioned within a distance of 100 Å. We applied FRET to measure interactions between the tetraspanins CD63 and CD82 as well as their interactions with MHC-II and HLA-DM. MVBs were expanded by chloroquine, which repositions molecules to the LM. The membranes required for expansion of the LM of MVBs are derived from ILV because MVBs still swell when vesicle transport is blocked by nocodazole, and ILV markers such as CD63 and CD82 appear at the LM of swollen MVBs. This implies that chloroquine somehow induces back-fusion of ILV. The molecular mechanism of this process is as yet unclear.

We first determined the interaction, expressed as E_D, between the tetraspanin proteins CD63 and CD82 when predominantly present at ILV (after 10 minutes of chloroquine) and LM (after 6 hours of chloroquine). The interaction between CD63 and CD82 appeared to be very stable (same E_D), whereas CD63–CD63 and CD82–CD82 pairs had lower E_D at the ILV of the MVB. This does not necessarily mean fewer protein–protein interactions, but could also reflect a different orientation of the proteins in the ILV than on the LM, as FRET does not distinguished between these options. The results imply that different tetraspanins interact within the MVB and that these interactions are dynamic at different MVB subdomains. This is illustrated by different E_D values for the CD63 and the CD82 pairs. The stable CD63–CD82 interaction might function as a core, enabling other CD63 and CD82 molecules to interact dynamically.

Although FRET resolves protein–protein interactions at a very high resolution, it is difficult to measure more than one pair using genetically encoded fluorophores. To study the interaction of HLA-DM or MHC-II with tetraspanins, we had to generate various cell lines. Again, we observed marked differences for tetraspanin interactions with MHC-II or HLA-DM within the MVB. MHC-II interacted stably with CD63, but only at the LM with CD82. HLA-DM interacted stably with CD82 whereas the MHC-II–CD63 pair showed strongest E_D at the LM of MVBs. In addition, HLA-DM and MHC-II preferentially interacted at the ILV within the MVB (Zwart et al., 2005).

It is unclear why tetraspanin pairs would reorganize at the ILV or LM of the MVB. The lipid and protein content of the two MVB subdomains is different. ILV concentrates the lipids LBPA and cholesterol (Kobayashi et al., 1998; Matsuo et al., 2004), which might contribute to the assembly of tetraspanin networks. Proteins are also unevenly distributed over the two MVB subdomains, as illustrated by the tetraspanins that accumulate in ILV (Escola et al., 1998). Finally, the curvature of ILV is definitively different from the curvature of the LM of the same MVB, which might affect formation of particular (lipid–)protein complexes (Mukherjee and Maxfield, 2000).

By applying FRET technology, we have shown for the first time that tetraspanin interactions, as well as interactions with other proteins such as MHC-II and HLA-DM, are dynamic within one subcellular structure. However, the tetraspanins do not

coach HLA-DM-mediated peptide loading. Rather, they affect expression of MHC-II at the plasma membrane as shown following silencing of CD63, but not CD82. CD63, unlike CD82, stably interacts with MHC-II at LM and ILV and might act as a co-chaperone, delaying release from the MVB until proper peptide loading has occurred. Alternatively, CD63 might trigger internalization of associated MHC-II at the cell surface until the latter is released by an as-yet-unknown mechanism. Whether the MHC-II peptide repertoire is affected by CD63 is at present unclear.

The observations from our FRET studies suggest that tetraspanin protein complexes reorganize at different locations within the MVB. This might define the release of proteins from the MVB, as suggested here for MHC-II, which is more efficiently expressed at the plasma membrane in the absence of CD63.

Materials and Methods

DNA constructs and the generation of transfectants

To generate pCFPC1-CD63 and pYFPC1-CD63, we retrieved CD63 from an GFP–CD63 fusion construct (Blott et al., 2001) using *Bam*HI-*Mlu*1 and placed CD63 into peCFP-C1 (Clontech), peYFP-C1 [pYFP-C1 was generated by exchange of CFP from peCFP-C1 for YFP (Miyawaki et al., 1997; van Rheenen et al., 2004)], pmCFP-C1 and pnCitrine-C1. To generate pCFPC1-CD82 and pYFPC1-CD82, CD82 was amplified from image clone 2959683 using CD82 forward primer 5′-GAAGATCTATGGGCTCAGCCTGTATCAAA-3′ and CD82 reversed primer 5′-CGGAATTCTCAGTACTTGGGGACCTTG-3′ and was ligated into peCFP-C1 and peYFP-C1 using *Bgl*II-*Eco*RI. pcDNA3-p31Ii was a kind gift from Oddmund Bakke (University of Oslo, Oslo, Norway) (Bakke and Dobberstein, 1990) pcDNA3.1 Zeo DMβ-IRES-DMα/YFP, pcDNA3 DRα-IRES-DR3β/CFP, pcDNA3-H2B/CFP and pcDNA3-H2B/YFP were already described (Zwart et al., 2005).

Antibodies

Monoclonal antibodies used were anti-CD63 (NKI-C3) (Vennegoor and Rumke, 1986), anti-CD82 (C33) (Fukudome et al., 1992; Imai et al., 1992), anti-HLA-DMA (5C1) (Sanderson et al., 1996), anti-LAMP2 (CD107b, BD Pharmingen), L243 and CerCLIP.1 and were isolated from hybridoma cell lines L243 (anti-HLA-DR complex, ATCC) and CerCLIP.1 (anti-CLIP24) as described previously (Lampson and Levy, 1980; Denzin et al., 1994). Rabbit polyclonal anti-GFP (Rocha et al., 2009), anti-HLA-DR (Neefjes et al., 1990) and anti-human CD63 (NKI-C3 serum) were used.

Cell lines

Cells were cultured in DMEM (Gibco) supplemented with 7.5% fetal calf serum (Gibco) in the presence or absence of 1000 μg/ml G418, 300 μg/ml Hygromycin (Gibco), 500 μg/ml Zeocine (Invitrogen) and/or 2 μM Ouabaine (Invitrogen) at 37℃ in a humidified atmosphere containing 5% CO_2. Stable and homogeneous expression of CFP- and YFP-tagged proteins was ensured by regular selection of CFP- and YFP-positive cells by fluorescence activated cell sorting (FACS). Stable transfectants of the melanoma cell line MelJuSo (H2B–CFP, H2B–YFP) were grown in IMDM (Gibco) medium with 7.5% fetal calf serum supplemented with 1000 μg/ml G418 (Gibco).

siRNA transfection, quantitative RT-PCR and flow cytometry

Gene silencing was performed in the human melanoma cell line MelJuSo using DharmaFECT transfection reagent #1 and 25 nM siRNA (Human siGenome SMARTpool library, Dharmacon) against CD63, CD81, KAI1, CD9, HLA-DMB and non-targeting control #1 (siControl). At 3 days post-transfection, cells were analyzed by quantitative RT-PCR. mRNA was extracted (mRNA Capture Kit) and reverse transcribed into cDNA (Transcriptor High Fidelity cDNA Synthesis Kit). The quantitative RT-PCR was performed using LightCycler 480 SYBR Green 1 Master on the LightCycler 480 Detection System (all Roche). Quantification was performed using the comparative C_T method ($\Delta\Delta C_T$). The results were expressed relative to GAPDH values, normalized to cells treated with control siRNA and LOG2-transformed. Primer sequences are listed in supplementary material Table S1.

At 6 days post-transfection, siRNA-transfected MelJuSo cells were analyzed by flow cytometry (BD FACSArray) using L243-Cy3 and CerCLIP-Cy5 monoclonal antibodies, as described (Paul et al., 2011). For microscopy, these cells were seeded on fibronectin-coated μ-Slide 18-well plates (flat ibiTreat, Ibidi). Cells were fixed with PBS containing 3.75% acid-free formaldehyde (Merck), permeabilized with PBS containing 0.1% Triton X-100 (Sigma) and blocked with PBS containing 0.5% bovine serum albumin (Sigma). Cells were stained with rabbit anti-HLA-DR (Neefjes et al., 1990), mouse anti-LAMP2 (CD107b, BD Pharmingen), goat anti-mouse–Alexa-Fluor-488 and goat anti-rabbit–Alexa-Fluor-647 (Invitrogen), washed with PBS and covered with 80% glycerol (Merck) in PBS. Stained cells were analyzed by a Leica TCS SP2 microscope with appropriate filters for fluorescence detection.

Flow cytometry of cell surface MHC class II

HEK293T cells transfected with the various constructs or MelJuSo cells were harvested from culture plates using trypsin–EDTA (Gibco) and collected in PBS supplemented with 2% fetal calf serum. Cells were incubated with primary antibodies L243 and CerCLIP.1 at 4℃ for 45 minutes. After two additional washes, cells were incubated with secondary antibody goat anti-mouse–Alexa-Fluor-647 (Invitrogen) at 4℃ for 30 minutes. After three washes, cells were analyzed by a FACS Calibur (Becton Dickinson).

CLSM and cryo-immuno-electron microscopy

For CLSM analysis, coverslips were coated with 5 μg/ml fibronectin (Sigma-Aldrich) in PBS for 1 hour at 37℃. Subsequently, HEK293T transfectants were seeded onto the coated coverslips. Cells were fixed by a 3.75% acid-free formaldehyde solution (Merck) in PBS and stained with anti-CD63 antibodies (NKI-C3) and anti-CD82 antibodies (C33) and secondary antibodies conjugated to goat anti-mouse–Alexa-Fluor-647. Images were taken with a Leica TCS SP2 System (Leica).

HEK293T transfectants were incubated with 200 μM chloroquine for 3 hours before processing. Cells were fixed in a mixture of paraformaldehyde (2%) and glutaraldehyde (0.2%) in 0.1 M PHEM buffer (60 mM PIPES, 25 mM HEPES, 2 mM MgCl2, 10 mM EGTA, pH 6.9) prior to processing for cryo-immuno-electron microscopy. For immunolabelling, sections were incubated with purified mAb anti-human DMα (5C1) or mAb anti-human CD82 (C33) and followed by incubations with rabbit anti-mouse IgG and protein A-conjugated 10 nm or 15 nm colloidal gold (EM Lab, Utrecht University, the Netherlands). For double labelling, the sections were fixed again for 10 minutes with 1% glutaraldehyde, followed by a second incubation with rabbit anti-GFP, rabbit anti-human HLA-DR serum or rabbit anti-human CD63 (NKI-C3) serum followed by labelling with protein A-conjugated 10 nm or 15 nm colloidal gold. After embedding in a mixture of methylcellulose and uranyl acetate, sections were analyzed in a Philips CM10 electron microscope (Philips, Eindhoven, the Netherlands).

FRAP

FRAP experiments were performed with a Leica TCS SP2 System with AOBS controlled emission using a 63× oil lens with a temperature controlled culture device. Focussing on the basal plasma membrane, a region of interest (ROI) was chosen and bleached at maximum power for 1 second at zoom four for one second, returning to 5% laser power for subsequent imaging. First, five pictures (at 512×512 pixel resolution) were taken at time intervals of 1.6 seconds to measure the fluorescence before bleaching (F_i). Then, a bleach-point was set in the middle of a cell. Reappearance of fluorescence until F_∞ in the bleach spot area was measured over a period of approximately 8 minutes.

The immobile fraction and the rate of mobility were determined from the fluorescence recovery curve. The rate of mobility is given by the diffusion time (t_D), which is the time-period required for recovery of 50% of the fluorescence of the mobile fraction. The immobile fraction (I) was calculated using the equation $I=(F_i-F_\infty)/F_i$, where F_i represents the fluorescence before bleaching and F_∞ the recovered fluorescence in the bleach spot area at infinite time after bleaching (Reits and Neefjes, 2001).

CLSM-FRET imaging for sensitized emission FRET

The HEK293T transfectants were grown on coated coverslips for 72 hours before imaging. At 16 hours prior to imaging, MelJuSo cells stably transfected with H2B–CFP or H2B–YFP (as internal calibration standards for leak-through and laser fluctuation), were added to the culture as detailed before (van Rheenen et al., 2004). Cells on coverslips were analyzed by CLSM in a heated tissue culture chamber at 37℃ and in a cooled tissue culture chamber at 19℃ under 5% CO_2. Prior to CLSM analysis, culture medium was exchanged for 3 ml of heated (37℃) or cooled (4℃) CBS medium (140 mM NaCl, 5 mM KCl, 2 mM $MgCl_2$, 1 mM $CaCl_2$, 23 mM $NaHCO_3$, 10 mM D-glucose, 10 mM HEPES pH 7.3). When indicated, chloroquine was added at a final concentration of 200 μM for 10 minutes, 3 hours or 6 hours prior to analyses. For the samples left untreated or incubated for 6 hours with chloroquine at 37℃, nocodazole (3 μM final concentration) was used to block intracellular vesicle motility.

FRET between CFP- and YFP-tagged molecules was studied by calculating the sensitized emission (the YFP emission upon CFP excitation) from separately acquired donor and acceptor images. Images were acquired on a DM-Ire2 inverted microscope fitted with a TCS-SP2 scanhead (Leica). Three images were collected: CFP was excited at 430 nm and detected between 470 and 490 nm; indirect YFP

was excited at 430 nm and detected between 528 and 603 nm; and direct YFP was excited at 514 nm and detected between 528 and 603 nm.

Because of considerable overlap of CFP and YFP spectra, YFP emission was corrected for leak-through of CFP emission and for direct excitation of YFP during CFP excitation using the co-cultured MelJuSo cells expressing only H2B–CFP or H2B–YFP as internal standards. FRET was calculated from these data as described in detail (van Rheenen et al., 2004). Sensitized emission (FSen) was calculated using correction factors obtained from cells expressing either CFP or YFP alone, which were updated for every image. Then, the donor FRET efficiency E_D was determined by relating the FSen to donor fluorescence level on a pixel-by-pixel basis.

Acknowledgements

We are grateful to K. Jalink for introducing us to confocal FRET measurements and for critical suggestions on the manuscript.

Funding

This study was supported by grants from the Dutch Cancer Foundation Koningin Wilhelmina Fonds (KWF); the Netherlands Organization for Scientific Research (NWO-ALW) [grant number 815.02.009]; and a European Research Council (ERC) Advanced Grant.

Supplementary material available online at
http://jcs.biologists.org/lookup/suppl/doi:10.1242/jcs.088047/-/DC1

References

Avva, R. R. and Cresswell, P. (1994). In vivo and in vitro formation and dissociation of HLA-DR complexes with invariant chain-derived peptides. *Immunity* **1**, 763-774.

Bakke, O. and Dobberstein, B. (1990). MHC class II-associated invariant chain contains a sorting signal for endosomal compartments. *Cell* **63**, 707-716.

Blott, E. J., Bossi, G., Clark, R., Zvelebil, M. and Griffiths, G. M. (2001). Fas ligand is targeted to secretory lysosomes via a proline-rich domain in its cytoplasmic tail. *J. Cell Sci.* **114**, 2405-2416.

Denzin, L. K. and Cresswell, P. (1995). HLA-DM induces CLIP dissociation from MHC class II alpha beta dimers and facilitates peptide loading. *Cell* **82**, 155-165.

Denzin, L. K., Robbins, N. F., Carboy-Newcomb, C. and Cresswell, P. (1994). Assembly and intracellular transport of HLA-DM and correction of the class II antigen-processing defect in T2 cells. *Immunity* **1**, 595-606.

Engering, A. and Pieters, J. (2001). Association of distinct tetraspanins with MHC class II molecules at different subcellular locations in human immature dendritic cells. *Int. Immunol.* **13**, 127-134.

Escola, J. M., Kleijmeer, M. J., Stoorvogel, W., Griffith, J. M., Yoshie, O. and Geuze, H. J. (1998). Selective enrichment of tetraspan proteins on the internal vesicles of multivesicular endosomes and on exosomes secreted by human B-lymphocytes. *J. Biol. Chem.* **273**, 20121-20127.

Fukudome, K., Furuse, M., Imai, T., Nishimura, M., Takagi, S., Hinuma, Y. and Yoshie, O. (1992). Identification of membrane antigen C33 recognized by monoclonal antibodies inhibitory to human T-cell leukemia virus type 1 (HTLV-1)-induced syncytium formation: altered glycosylation of C33 antigen in HTLV-1-positive T cells. *J. Virol.* **66**, 1394-1401.

Griffiths, G., Hoflack, B., Simons, K., Mellman, I. and Kornfeld, S. (1988). The mannose 6-phosphate receptor and the biogenesis of lysosomes. *Cell* **52**, 329-341.

Gromme, M., Uytdehaag, F. G., Janssen, H., Calafat, J., van Binnendijk, R. S., Kenter, M. J., Tulp, A., Verwoerd, D. and Neefjes, J. (1999). Recycling MHC class I molecules and endosomal peptide loading. *Proc. Natl. Acad. Sci. USA* **96**, 10326-10331.

Hammond, C., Denzin, L. K., Pan, M., Griffith, J. M., Geuze, H. J. and Cresswell, P. (1998). The tetraspan protein CD82 is a resident of MHC class II compartments where it associates with HLA-DR, -DM, and -DO molecules. *J. Immunol.* **161**, 3282-3291.

Imai, T., Fukudome, K., Takagi, S., Nagira, M., Furuse, M., Fukuhara, N., Nishimura, M., Hinuma, Y. and Yoshie, O. (1992). C33 antigen recognized by monoclonal antibodies inhibitory to human T cell leukemia virus type 1-induced syncytium formation is a member of a new family of transmembrane proteins including CD9, CD37, CD53, and CD63. *J. Immunol.* **149**, 2879-2886.

Kobayashi, T., Stang, E., Fang, K. S., de Moerloose, P., Parton, R. G. and Gruenberg, J. (1998). A lipid associated with the antiphospholipid syndrome regulates endosome structure and function. *Nature* **392**, 193-197.

Kropshofer, H., Arndt, S. O., Moldenhauer, G., Hammerling, G. J. and Vogt, A. B. (1997). HLA-DM acts as a molecular chaperone and rescues empty HLA-DR molecules at lysosomal pH. *Immunity* **6**, 293-302.

Lampson, L. A. and Levy, R. (1980). Two populations of Ia-like molecules on a human B cell line. *J. Immunol.* **125**, 293-299.

Matsuo, H., Chevallier, J., Mayran, N., Le Blanc, I., Ferguson, C., Faure, J., Blanc, N. S., Matile, S., Dubochet, J., Sadoul, R. et al. (2004). Role of LBPA and Alix in multivesicular liposome formation and endosome organization. *Science* **303**, 531-534.

Min, G., Wang, H., Sun, T. T. and Kong, X. P. (2006). Structural basis for tetraspanin functions as revealed by the cryo-EM structure of uroplakin complexes at 6-A resolution. *J. Cell Biol.* **173**, 975-983.

Miyawaki, A., Llopis, J., Heim, R., McCaffery, J. M., Adams, J. A., Ikura, M. and Tsien, R. Y. (1997). Fluorescent indicators for Ca2+ based on green fluorescent proteins and calmodulin. *Nature* **388**, 882-887.

Mukherjee, S. and Maxfield, F. R. (2000). Role of membrane organization and membrane domains in endocytic lipid trafficking. *Traffic* **1**, 203-211.

Neefjes, J. (1999). CIIV, MIIC and other compartments for MHC class II loading. *Eur. J. Immunol.* **29**, 1421-1425.

Neefjes, J. J., Stollorz, V., Peters, P. J., Geuze, H. J. and Ploegh, H. L. (1990). The biosynthetic pathway of MHC class II but not class I molecules intersects the endocytic route. *Cell* **61**, 171-183.

Paul, P., van den Hoorn, T., Jongsma, M. L., Bakker, M. J., Hengeveld, R., Janssen, L., Cresswell, P., Egan, D. A., van Ham, M., Ten Brinke, A. et al. (2011). A genome-wide multidimensional RNAi screen reveals pathways controlling MHC class II antigen presentation. *Cell* **145**, 268-283.

Peters, P. J., Neefjes, J. J., Oorschot, V., Ploegh, H. L. and Geuze, H. J. (1991). Segregation of MHC class II molecules from MHC class I molecules in the Golgi complex for transport to lysosomal compartments. *Nature* **349**, 669-676.

Reits, E. A. and Neefjes, J. J. (2001). From fixed to FRAP: measuring protein mobility and activity in living cells. *Nat. Cell Biol.* **3**, E145-E147.

Rocha, N., Kuijl, C., van der Kant, R., Janssen, L., Houben, D., Janssen, H., Zwart, W. and Neefjes, J. (2009). Cholesterol sensor ORP1L contacts the ER protein VAP to control Rab7-RILP-p150 Glued and late endosome positioning. *J. Cell Biol.* **185**, 1209-1225.

Roche, P. A. and Cresswell, P. (1990). Invariant chain association with HLA-DR molecules inhibits immunogenic peptide binding. *Nature* **345**, 615-618.

Rubinstein, E., Le Naour, F., Lagaudriere-Gesbert, C., Billard, M., Conjeaud, H. and Boucheix, C. (1996). CD9, CD63, CD81, and CD82 are components of a surface tetraspan network connected to HLA-DR and VLA integrins. *Eur. J. Immunol.* **26**, 2657-2665.

Saffman, P. G. and Delbruck, M. (1975). Brownian motion in biological membranes. *Proc. Natl. Acad. Sci. USA* **72**, 3111-3113.

Sanderson, F., Thomas, C., Neefjes, J. and Trowsdale, J. (1996). Association between HLA-DM and HLA-DR in vivo. *Immunity* **4**, 87-96.

Tarrant, J. M., Robb, L., van Spriel, A. B. and Wright, M. D. (2003). Tetraspanins: molecular organisers of the leukocyte surface. *Trends Immunol.* **24**, 610-617.

Teis, D., Saksena, S. and Emr, S. D. (2009). SnapShot: the ESCRT machinery. *Cell* **137**, 182-182.e181.

Unternaehrer, J. J., Chow, A., Pypaert, M., Inaba, K. and Mellman, I. (2007). The tetraspanin CD9 mediates lateral association of MHC class II molecules on the dendritic cell surface. *Proc. Natl. Acad. Sci. USA* **104**, 234-239.

van Rheenen, J., Langeslag, M. and Jalink, K. (2004). Correcting confocal acquisition to optimize imaging of fluorescence resonance energy transfer by sensitized emission. *Biophys. J.* **86**, 2517-2529.

Vennegoor, C. and Rumke, P. (1986). Circulating melanoma-associated antigen detected by monoclonal antibody NKI/C-3. *Cancer Immunol. Immunother.* **23**, 93-100.

Wang, H. X., Kolesnikova, T. V., Denison, C., Gygi, S. P. and Hemler, M. E. (2011). The C-terminal tail of tetraspanin protein CD9 contributes to its function and molecular organization. *J. Cell Sci.* **124**, 2702-2710.

Wubbolts, R., Leckie, R. S., Veenhuizen, P. T., Schwarzmann, G., Mobius, W., Hoernschemeyer, J., Slot, J. W., Geuze, H. J. and Stoorvogel, W. (2003). Proteomic and biochemical analyses of human B cell-derived exosomes. Potential implications for their function and multivesicular body formation. *J. Biol. Chem.* **278**, 10963-10972.

Zwart, W., Griekspoor, A., Kuijl, C., Marsman, M., van Rheenen, J., Janssen, H., Calafat, J., van Ham, M., Janssen, L., van Lith, M. et al. (2005). Spatial separation of HLA-DM/HLA-DR interactions within MIIC and phagosome-induced immune escape. *Immunity* **22**, 221-233.

Journal of Cell Science

Table S1. Primers used in this study

	Forward	Reverse
CD63	5′-GATCACGTTTGCCATCTTTCTGTC-3′	5′-TGACATCACCTTATCTCTAAACACATAGCC-3′
CD81	5′-TTCCACGAGACGCTTGACTG-3′	5′-CTGATGATGTTGCTGCCCGA-3′
CD82	5′-GCTCAGCCTGTATCAAAGTCAC-3′	5′-GAGGAGGTTTGCAGGACAGAG-3′
CD9	5′-AACGCTGAAAGCCATCCAC-3′	5′-CATCAGGACAGGACTTCACGG-3′
HLA-DMB	5′-CCAGCCCAATGGAGACTG-3′	5′-CAGCCCAGGTGTCCAGTC-3′
HLA-DRA	5′-CATGGGCTATCAAAGAAGAAC-3′	5′-CTTGAGCCTCAAAGCTGGC-3′
GAPDH	5′-GGTGCTAAGCAGTTGGTGGTG-3′	5′-CCATGTTCGTCATGGGTGTG-3′.